Journal of Korean Magnetics Society, Volume 5, Number 5, October 1995

# MICROMAGNETISM OF HARD AND SOFT MAGNETIC MATERIALS

**Helmut Kronmüller**

**Max-Planck-Institut für Metallforschung, Institut für Physik, Heisenbergstraße 1, D-70569 Stuttgart, Germany**

*Abstract*-High performance magnetic materials are characterized by the combination of outstanding magnetic properties and optimized microstructures, e.g., nanocrystalline composites of multilayers and small particle systems. The characteristic parameters of the hysteresis loops of these materials vary over more than a factor of $10^6$ with optimum values for the coercive field of several Tesla and permeabilities of $10^6$. Within the framework of the computational micromagnetism (nanomagnetism) using the finite element method the upper and lower bounds of the coercive field of different types of grain ensembles and multilayers have been determined. For the case of nanocrystalline composites the role of grain size, exchange and dipolar coupling between grains and the degree of grain alignment will be discusses in detail. It is shown that the largest coercivities are obtained for exchange decoupled grains, whereas remanence enhancing requires exchange coupled grains below 20 nm. For composite permanent magnets based on $Nd_2Fe_{14}B$ with an amount of ~ 50% soft α-Fe-phase coercivities of $\mu_0 H_c = 0.75$ T, a remanence of 1.5 T and an energy product of 400 kJ/m$^3$ is expected.

In nanocrystalline systems the temperature dependence of the coercivity is well described by the relation $\mu_0 H_c = (2\,K_1/M_s)$ $\alpha - N_{eff}\mu_0 M_s$, where the microstructural parameters α and $N_{eff}$ take care of the short-range perturbations of the anisotropy and $N_{eff}$ is related to the long-range dipolar interactions. $N_{eff}$ is found to follow a logarithmic grain size dependence $\mu_0 H_c = (2\,K_1/M_s)$ $\alpha - N_{eff}(\beta \ln D)\mu_0 M_s$. Several trends how to achieve the ideal situation $\alpha \to 1$ and $N_{eff} \to 1 \to 0$ will be discussed.

## I. INTRODUCTION

The rise of high-quality permanent magnets started with the discovery of the intermetallic compound $SmCo_5$ followed by $Sm_2Co_{17}$ [1-4], $Nd_2Fe_{14}B$ and $Sm_2Fe_{17}N_{3-x}$ [5-7]. The success of these rare earth magnets is based on their outstanding intrinsic properties but also on the developments of special microstructures. The techniques of sintering, rapid quenching from the melt, mechanical alloying [8] and the hydrogen descrepitation method [9] has opened the possibility to produce a wide spectrum of microstructures which allow the tailoring of the characteristic properties of the hysteresis loop. Recently, the development of nanocrystalline materials has become of special interest for the improvement of hard as well as of soft magnetic materials [10, 11, 12]. In the case of hard magnetic materials the nanocrystalline state can be used to enhance the remanence of isotropic materials, whereas in the case of soft magnetic materials an enhancement of the permeability can be achieved making use of the random anisotropy effect.

The micromagnetic backgrounds of these controversial effects will be the topic of this paper.

## II .CHARACTERISTIC PROPERTIES OF THE HYSTERESIS LOOP

Ferromagnetic materials are characterized by their hysteresis loop and the initial magnetization curve. For soft as well as hard magnetic materials the main properties are the remanent polarization $J_r = \mu_0 M_r$, ($\mu_0 = 4\pi \cdot 10^{-7}$ (Vs/Am) vacuum permeability, $M_r$ = remanent magnetization), the coercive field $H_c$, and the initial magnetization curve described by the so-called Rayleigh law

$$M(H) = \chi_0 H + \alpha_R H^2 \qquad (1)$$

which holds for $H < 0.5\,H_c$ and where $\chi_0$ denotes the initial susceptibility and $\alpha_R$ the Rayleigh constant.

Another important quantity characterizing hard magnetic materials is the so-called maximum energy product

$$(BH)_{max} = \frac{1}{4}\mu_0 M_r^2 \qquad (2)$$

which corresponds to the stored magnetic energy of the permanent magnet. The coercive field may be considered as the main property of the hysteresis loop which varies from 0.1 A/m in high-permeability materials up to several $10^6$ A/m. $H_c$ depends on the intrinsic material constants (spontaneous magnetization $M_s$, anisotropy constant, $K_1$ exchange constant, A) and the microstructure. As shown in Fig. 1 the coercive field of different types of material groups increases linearly with $K_1$. In all these types of materials the coercive field is well described by the relation [13]

$$H_c = \frac{2K_1}{\mu_0 M_c}\alpha - N_{eff} M_s\,, \qquad (3)$$

where α and Neff are microstructural parameters. Here, α takes care of regions with reduced anisotropy constant at grain surfaces and to misligned grains. The term $-N_{eff}M_s$ corresponds to an average local demagnetization field resulting from magnetic surface charges.

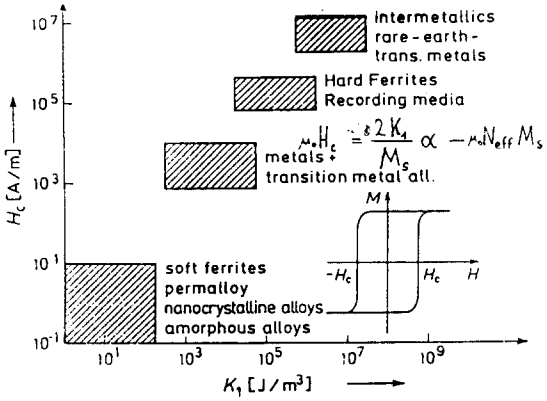


Fig. 1 Schematic representation of coercive fields of soft and hard magnetic materials as a function of $K_1$.

## III. MICROSTRUCTURAL PARAMETERS AND MICROMAGNETIC PHASE DIAGRAM OF PERMANENT MAGNETS

The maximum energy product $(BH)_{max}$ can only be realized if the condition $H_c > 0.5\, M_r$ holds and if a rectangular hysteresis loop exists. It is therefore of interest to determine the range of parameters $\alpha$ and $N_{eff}$ where this condition holds. For establishing a phase diagram we take into account that $\alpha$ according to $\alpha = \alpha_\psi \cdot \alpha_K$ is composed of two factors, where $\alpha_\psi$ takes care of misaligned grains and $\alpha_K$ of deteriorated grain surfaces with reduced anisotropies. The minimum value of $\alpha_\psi^{min}$ is of the order of 0.5 for grains misaligned by $\pi/4$. According to Fig. 2 the parameters $\alpha_K$ and $N_{eff}$ may be determined from a plot [13, 14]

$$H_c/M_s \text{ vs. } \frac{2K_1}{\mu_0 M_s^2}\alpha_\psi^{min} \qquad (4)$$

Since $(2K_1/\mu_0 M_s^2)\alpha_\psi^{min}$ as a function of temperature varies over a wide range, the plot (4) allows a determination of $\alpha_K$ and $N_{eff}$ if this plot leads to a linear relation. Fig. 2 shows a series of such plots for sintered, mechanically alloyed and rapidly quenched permanent magnets revealing a linear behaviour between 25 K and 500 K for FePrB alloys. In the case of $Nd_2Fe_{14}B$ deviations are observed in the temperature range below 180 K resulting probably from a significant temperature dependence of the $\alpha_K$ parameter.

Setting $H_c = kM_s$ eq. (3) may be rearranged as follows

$$\alpha_K = \frac{\mu_0 M_s^2}{\left(2K_1\alpha_\psi^{min}\right)}(k + N_{eff}) \qquad (5)$$

Fig. 2 Analysis of the temperature dependence of Hc by means of eq. (4).

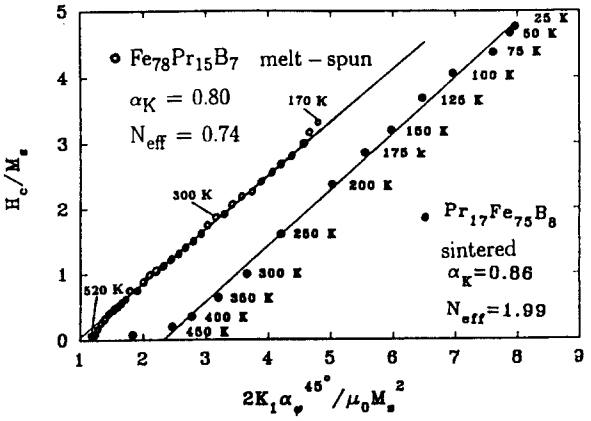


a) Melt-spun $Pr_{15}Fe_{78}B_7$ and sintered $Pr_{15}Fe_{78}B_8$.

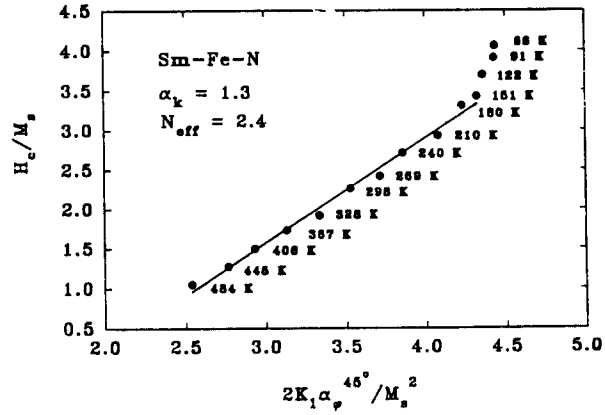


b) Mechanically alloyed $Sm_2Fe_{17}N_x$.

For the material parameters of $Nd_2Fe_{14}B$ ($\mu_0 M_s = 1.61$ T, $K_1 = 4.3 \cdot 10^6$ J/m³, $\alpha_\psi^{min} = 0.5$) we find $\alpha_K = 0.48\,(k + N_{eff})$. Since in magnets with deteriorated grain surfaces $\alpha_K$ cannot exceed a maximum value of $\alpha_K = 1$, the allowed values of $\alpha_K$ and $N_{eff}$ lie in the shaded triangle shown in Fig. 3. Most of the experimental results lie within the triangle for $k = 0.5$. It should be noted, however, that $k = 0.5$ corresponds to the lower allowable bound of $H_c$ if a perfect rectangular low hysteresis loop exists. Actually, this situation cannot be realized for real permanent magnets and the condition $k = 0.75$ guarantees the use of $(BH)_{max}$ much better. The reduced range of allowable $\alpha_K$-and $N_{eff}$-values is shown by the broken line in Fig. 3. It is of interest to note that for critical values $N_{eff} > 1.20$ the condition $H_c = 0.75\, M_s$ cannot be fulfilled. The microstructural parameters depend sensitively on the special properties of the microstructure of grain boundaries, grain size and phase distributions which will be discussed in detail in the following sections.

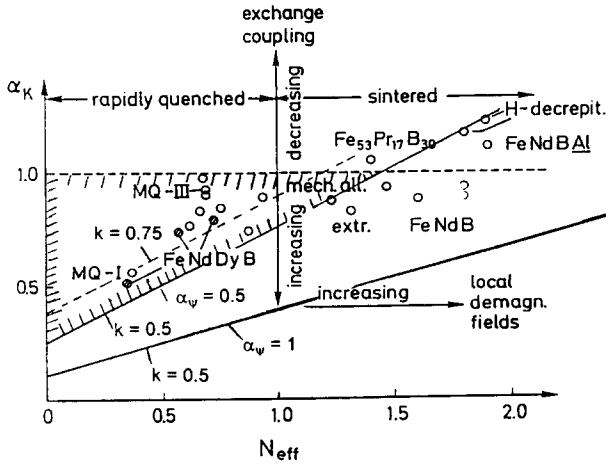


Fig. 3 Phase diagramme of the microstructural parameters $\alpha_K$, $N_{eff}$ for k = 0.5; 0.75. The shaded regions include all parameter combinations allowing the use of the maximum energy product in the case of a rectangular hysteresis loop. The experimental results refer to melt-spun, sintered and HD materials. Values $\alpha_K > 1$ indicate an underestimate of $a_\psi$.

## IV. HIGH-COERCIVE AND HIGH-REMANENCE MAGNETS

The drastic deviations of the experimentally realized coercive fields from the ideal nucleation field $H_N = 2K_1 / \mu_0 M_s^2$ ($\alpha = 1$, $N_{eff} = 0$) has to be attributed to imperfect grain surfaces and to the magnetic coupling between neighbouring grains. In order to achieve high-quality magnets the tailoring of the microstructure by suitable additives and by special production techniques has become the leading tool for developing high-tech permanent magnets [15].

1. High-coercivity magnets are obtained by two types of additives. Type I additives such as Dy, Pr, Co, Al are substitutionally dissolved in $Nd_2Fe_{14}B$ and modify the intrinsic material parameters suitably. E.g., Dy reduces $M_s$ and increases $K_1$ which both lead to an increase of $H_c$. Type II additives as Ga, Al, Cu increase the viscosity of the intergranular liquid phase during sintering and lead to a better magnetic decoupling between the grains. Type III additives such as Nb, V, Mo lead to the formation of high-melting borides, which act as barriers of grain growth during sintering. Type II as well as Type III additives in addition improve the corrosive properties of the Nd-rich intergranular phase. Characteristic compositions are $Fe_{74}Nd_{18}B_6Ga_1Nb_1$.
2. High-remanence magnets are obtained by rather stoichiometric compositions containing only a small amount of additives as e.g., $Ga_1Nb_1$. A further very promising technique to increase the remanence, and as a consequence also the energy product, are composite materials where hard magnetic grains are mixed with soft magnet grains of α-Fe. These composite materials require nanocrystalline microstructures where the grains are coupled by exchange interactions.
3. High-coercivity – High-Remanence magnets may be obtained by a compromise between the amount of additives and stoichiometry. In the case of nanocrystalline materials produced by melt-spinning or mechanical alloying exchange-enhanced remanences can be produced which lie 50% above the remanence of an isotropic distribution of grains still keeping a coercive field of ~ 1 Tesla.

## V. FRONTIERS OF NANOCRYSTALLINE COMPOSITES OF HARD MAGNETIC MATERIALS

### V.1 The role of exchange and dipolar coupling

The drastic deviation of $H_c$ from the ideal nucleation field is due to the combined action of deteriorated grain surfaces and magnetic coupling between the grains. Whereas imperfect grain surfaces can be widely eliminated by annealing treatments, the magnetic coupling between the grains cannot be suppressed. By means of finite element calculations [16] the magnetization processes of ensembles of grains have been investigated for different types of couplings:

1. Only dipolar long-range coupling between grains which are separated by a non-magnetic Nd-rich phase.
2. Only exchange coupled grains.
3. Exchange and dipolar coupling between grains.

The demagnetization curves of an ensemble of hexagonal two-dimensional grains with a statistical distribution of easy directions are shown in Fig. 4. Largest coercive field and

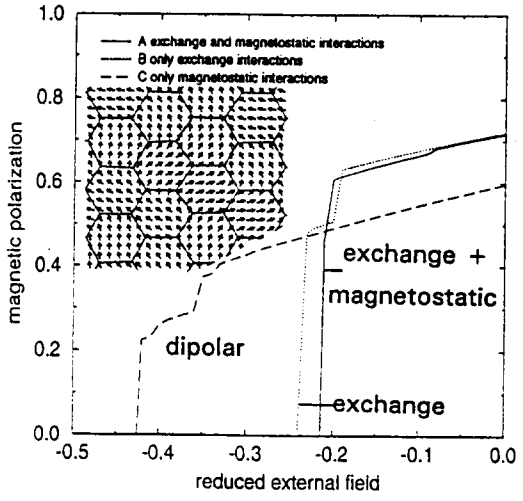


Fig. 4 Demagnetization curves for a two-dimensional isotropic distribution of easy directions and hexagonal Nd2Fe14B grains of diameter 15 nm. (—) Exchange and dipolar coupling, (····) only exchange coupling, (---) only magnetostatic, dipolar interactions. External field in units of $2K_1/J_s$ and magnetic polarization in units of $J_s = \mu_0 M_s$ [16].

smallest remanence is obtained for grains coupled only by dipolar stray fields. Largest remanence and lowest coercive field are obtained for exchange and dipolar coupled grains and an intermediate situation holds for only exchange coupled grains.

### V.2 Three-Dimensional Nanocrystalline Composite Magnets ($Nd_2Fe_{14}B$ and α-Fe)

Fig. 5 shows the spin arrangement of irregular grains with an amount of 51% of magnetically soft α-Fe grains [15]. The finite element calculations have been performed for full dipolar and exchange coupled grains. Regular as well as irregular grain ensembles have been considered. It turned out that the regular grain structures in general lead to

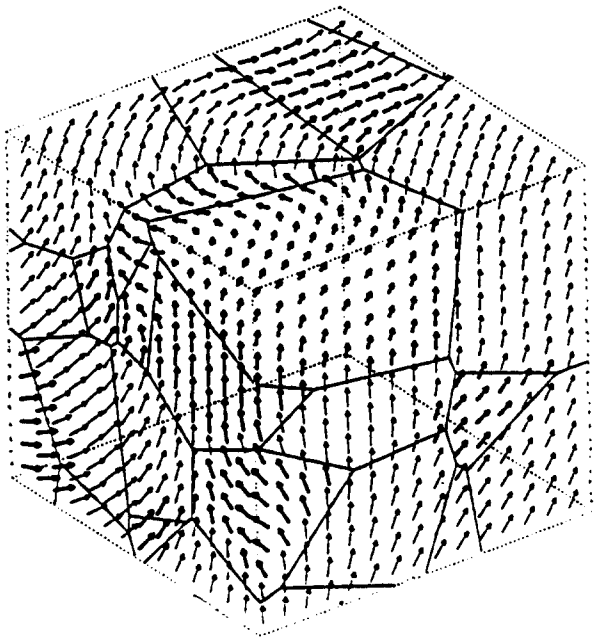

Fig. 5 Grain and spin structure of the remanent state for 35 irregular grains (D = 10 nm) with a volume fraction of 49% of magnetically hard grains (strong arrows, $Nd_2Fe_{14}B$) and 51% magnetically soft grains (weak arrows, α-Fe).

larger coercive fields. As an example Fig. 6 shows the demagnetization curves for a regular and an irregular grain structure of an average grain diameter D = 10 nm. The characterisitc parameters of the hysteresis loops $J_r$, $\mu_0 H_c$ and $(BH)_{max}$ as determined for the irregular two-phase grain structure of Fig. 5 are shown in Fig. 7 [17] for different amounts of the soft magnetic α-Fe and an average grain diameter of 10 nm. Here it has been assumed full exchange coupling between the grains.

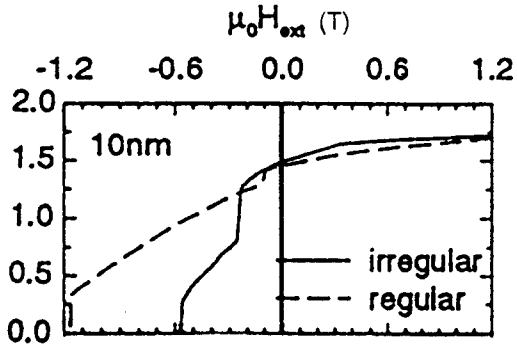


Fig. 6 Demagnetization curves of 35 regular or irregular grains with a volume fraction of 49% hard magnetic grains and a grain size of 10 nm.

Fig. 7 also contains the results for non-interacting Stoner-Wohlfarth particles. As it is expected due to the exchange coupling the remanence, $J_r$, is increased even for a vanishing α-Fe content. There exists a cross-over at around 50% soft phase where the condition $H_c = M_r/2$ holds. As mentioned in Section 2 this condition is required in order to make use of the maximum energy product $(BH)_{max}$. For an amount of 40% α-Fe the energy product is of the order of 400 kJ/m³ and the coercive field still is appreciable with 0.8 Tesla.

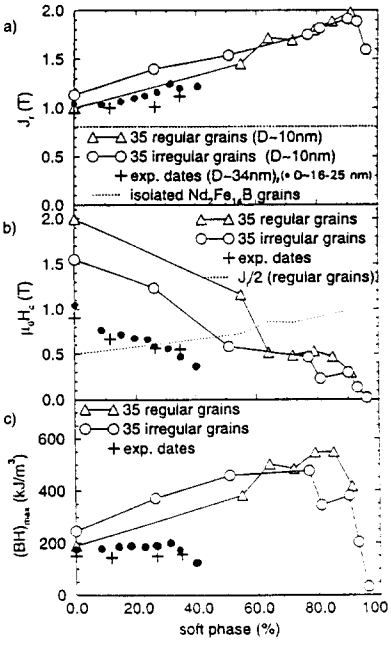


Fig. 7 $J_r$, $\mu_0 H_c$ and $(BH)_{max}$ of a regular and an irregular grain structure as a function of grain size for different amounts of magnetically soft phase and D = 10 nm. Coercivity of the regular grain structures exceeds that of the irregular grain structure. (+ [18]; • [19].

Fig. 7 also contains experimental results due to Wilcox et al. [18] and Bauer [19]. The experimental results obtained for melt-spun materials in the case of the remanence fit rather well with the theoretical predictions, whereas the experimental results for $\mu_0 H_c$ and $(BH)_{max}$ lie below the theoretical predictions. Nevertheless the qualitative behaviour of the coercive field agrees with the theoretical predictions. In the case of the experimental results the condition $H_c > M_r/2$ is valid up to 25% soft magnetic phase. Further improvements require larger coercive fields.

Another important material parameter is the effect of the grain size on magnetic properties. Fig. 8 presents the grainsize dependence of $J_r$, $H_c$ and $(BH)_{max}$ for 0%, 55% and 72% α-Fe. Fig. 8 also contains the experimental results obtained by Manaf et al. [20] for $Nd_{13.2}Fe_{79.2}B_6Si_{1.2}$. Excellent agreement is observed for the remanence, whereas the coercive field shows only qualitative agreement, however, agrees with the predicted decrease of $H_c$ for grains sizes below the wall width of α-iron.

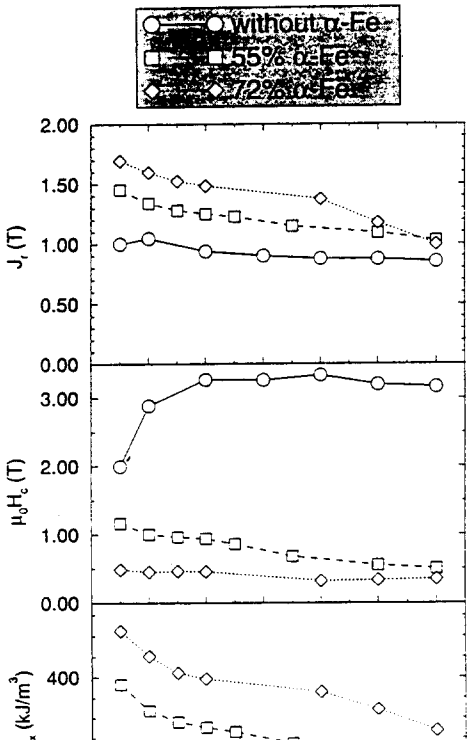


Fig. 8 $J_r$, $\mu_0 H_c$ and $(BH)_{max}$ of a regular grain structure as a function of grain size for different amounts of magnetically soft phase [17].

A quantitative description of the numerical results for $H_c$ and $J_r$ leads to lnD-laws:

$$H_c = H_N^{(O)}(0.22 - 0.41\ \ln D/\delta_B^{hard})$$
$$J_r = J_{sat}(0.84 - 0.085 \ln D/\delta_B^{hard}), \quad (6)$$

with $H_N^{(O)} = 2K_1/\mu_0 M_s$ and $J_{sat} = J_S^{hard}\ v^{hard} + J_S^{soft}\ v^{soft}$, where the upper indexes refer to the polarization and volume fractions of the hard and soft magnetic phase. $\delta_B^{hard}$ denotes the wall width of the hard magnetic phase (4.2 nm).

## VI. NANOCRYSTALLINE SOFT MAGNETIC MATERIALS

Promising soft magnetic materials (smm) have permeabilities up to $10^6$ and have been developed for quite different microstructures: crystalline, nanocrystalline and amorphous structures. For high-tech smm three conditions should be realized: (1) Low effective magnetic magnetostriction and high remanence, (2) Small magnetostriction, (3) Low conductivity and small domain widths to reduce the magnetic losses. An effective method of suitable intrinsic magnetic and microstructural properties.

Well-known examples are permalloys (Fe, Ni)-alloys and Fe-Si-transformer steel, where the intrinsic properties, $K_1$, and $\lambda_s$, are minimized by the chemical composition.

Excellent high-frequency materials are the nonmagnetostrictive amorphous alloys of type $(CoFe)_{70}$ $(MoSiB)_{30}$. Nanocrystalline materials produced by nanocrystallization from amorphous FeNbCuSiB alloys are suitable for higher temperatures than the metastable amorphous alloys [12, 21]. The small additives of Cu and Nb are responsible for a high density of crystallization nuclei and the prevention of the growing of large grains, respectively.

In the case where domain wall (dw) displacements or rotation processes govern the magnetization process $H_c$ and $\chi$ are related by an universal relation [22]

$$\chi H_c \cong \begin{cases} M_s\delta_B/D_0 & \text{(dw displacement)} \\ 0.85 & \text{(rotation)} \end{cases} \quad (7)$$

Here $\delta_B = \pi(A/K_1)^{1/2}$ denotes the dw width and $D_0$ the average dw distance. Fig. 9 gives a review of the above $\chi$-$H_c$-relation for different conventional amorphous alloys showing that the range within which some alloys exist is given by the parameter range $0.1\ A/cm \le M_s\delta_B/D_0 \le 10\ A/cm$. Fig. 9 also contains the absolute maximum and minimum of $\chi(> 10^6)$, respectively $H_c(> 10^{-5}\ A/cm)$ as obtained for nonmagnetostrictive ideal amorphous alloys. The nc alloys lie outside the above parameter range because in

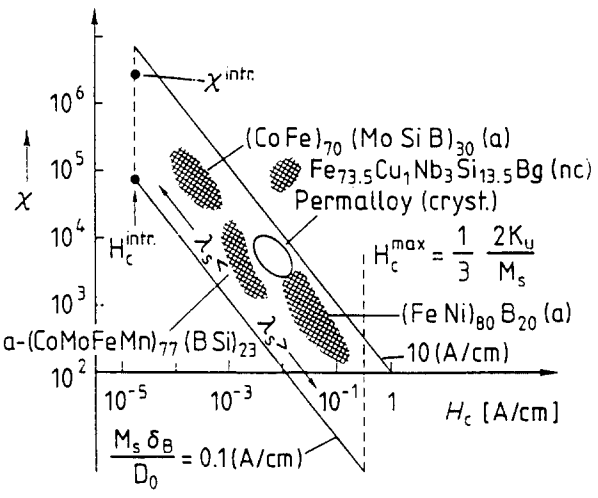


Fig. 9 $\chi$ versus $H_c$ for crystalline (c), nanocrystalline (nc) and amorphous (a) soft magnetic materials. The nc materials are beyond the upper border line (10 A/cm) because of its large domain wall width.

these alloys $\delta_B$ is given by $\langle\delta_B\rangle = \pi(A/\langle K_1\rangle)^{1/2}$. $\langle K_1\rangle$ denotes the effective anisotropy constant as derived from the random anisotropy model [21], and is given by $\langle K_1\rangle$ $K_1^4 D^6/A^3$. With the intrinsic material parameters of $Fe_3Si$ ($K_1 = 8000$ J/m$^3$, $A = 10^{-11}$ J/m), a grain size of 12 nm and a domain width of $D_0 = 350$ µm [23] we obtain $\langle\delta_B\rangle = 2.7$ µm and $\chi H_c/M_s = 8 \cdot 10^{-3}$. The drastic dependence of the latter quantity is shown in Fig. 10. Whereas in the amorphous

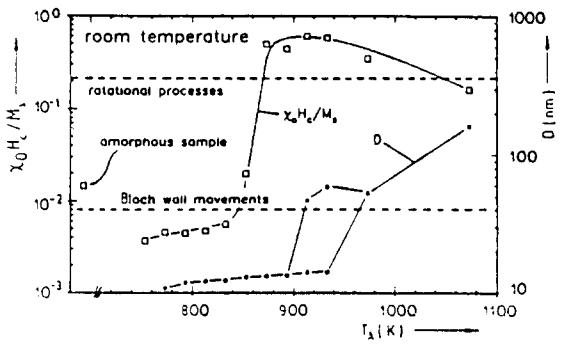


Fig. 10 Analysis of magnetization processes by the quantity $\chi H_c/M_s$ as a function of $T_A$ and grain size D.

and the nc structure up to D = 15 nm dw displacements govern the magnetization process, for D > 15 nm a transition to rotational processes takes place. Above an annealing temperature of 940 K $H_c\chi/M_s$ again decreases because in the range $D > \delta_B$ dw bowing contributes to the magnetization process. This interpretation of the change of magnetization processes is supported by the drastic decrease of the Rayleigh constant by six orders of magnitude [23].

## REFERENCES


[1] K.J. Strnat, J. Magn. Magn. Mat. 7, 351 (1978).

[2] R.K. Mishra, G. Thomas, T. Yoneyama, A. Tukono and T. Ojima, J. Appl. Phys. 52, 2517 (1981).

[3] G.C. Hadjipanayis, E.J. Yadlowsky and S.H. Wallins, J. Appl. Phys. 53, 2386 (1982).

[4] K.H.J. Buschow, in Ferromagnetic Materials, eds. K.H.J. Buschow and E.P. Wohlfarth (Elsevier, Amsterdam, 1988) Vol. 5, p.1.

[5] J.J. Croat, J.E. Herbst, R.W. Lee and F.E. Pinkerton, J. Appl. Phys. 55, 2078 (1984).

[6] M. Sagawa, S. Fujimura, N. Togawa, H. Yamamoto and G. Matsuura, J. Appl. Phys. 55, 2083 (1984).

[7] J.D. Coey and H. Sun, J. Magn. Magn. Mat. 87, L 251 (1990).

[8] K. Schnitzke, L. Schultz, J. Wecker and M. Katter, Appl. Phys. Letters 57, 2853 (1990).

[9] F.M. Ahmed, D.S. Edgley and I.R. Harris, in 13th International Symposium on Rare Earth Magnets and their Applications, Birmingham 1994, p. 463.

[10] J. Ding, G. Liu, P.G. McCormick and R. Street, J. Magn. Magn. Mat. 123, L 239 (1993), 124, 1 (1993).

[11] R. Skomski and J. Coey, IEEE Trans. Mag. MAG 29, 2860 (1993).

[12] Y. Yoshizawa and K. Yamauchi, IEEE Trans. Mag. MAG 26, 1397 (1990).

[13] H. Kronmüller, K.D. Durst and M. Sagawa,. J. Magn. Magn. Mat. 74, 291 (1988).

[14] H. Kronmüller, K.D. Durst, S. Hock, and G. Martinek, J. de Physique C8-49, 623 (1988).

[15] H. Kronmüller, in 8th International Symposium on Magnetic Anisotropy and Coercivity in Rare-Earth–Transition Metal Alloys, Birmingham 1994, p.1.

[16] T. Schrefl, J. Fidler and H. Kronmüller, Phys. Rev. B 49, 6100 (1994).

[17] R. Fischer, T. Schrefl, H. Kronmüller, and J. Fidler, J. Magn. Magn. Mat., to be published

[18] M. Wilcox, J. Williams, M. Leonowicz, A. Manaf and H. Davies, ibid. [15], p. 443.

[19] J. Bauer, private communication 1995.

[20] A. Manaf, R.A. Buckley, H.-A. Davies and M. Leonowicz, J. Magn. Magn. Mat. 101, 360 (1991).

[21] G. Herzer, IEEE Trans Mag. MAG 26, 1397 (1990).

[22] H. Kronmüller and T. Reininger, J. Mag. Mag. Mag. 112, 1 (1992).

[23] B. Hofmann, T. Reininger and H. Kronmüller, phys. stat. sol. (a) 134, 247 (1992).